Catalysis Today, 14 (1992) 293–303
Elsevier Science Publishers B.V., Amsterdam

In-situ pore structure characterization during sol-gel synthesis of controlled porosity materials

D. M. Smith[a], R. Deshpande[a], C.J. Brinker[a,b], W.L. Earl[c], B. Ewing[c], and P.J. Davis[a,c]

[a] UNM/NSF Center for Micro-Engineered Ceramics, University of New Mexico, Albuquerque, NM, 87131

[b] Sandia National Laboratories, Albuquerque, NM, 87185

[c] Los Alamos National Laboratory, Los Alamos, NM, 87545

Abstract

Using NMR relaxation measurements of pore fluid, the pore volume, surface area, and pore size distribution of wet materials may be measured in-situ. In this manner, changes in pore structure may be directly observed during various aging steps (i.e., temporal, thermal, solvent exchange, pH) of sol-gel derived porous solids. By combining these relaxation measurements with Nuclear Magnetic Resonance Imaging (NMRI), the **spatial variation of pore structure** may be observed. In addition to how the surface area, porosity, and pore size distribution vary at different points within the sample, the change of sample physical dimensions during processing can be measured. This enables the study of catalyst-related problems such as "skin" effects and catalyst supports with spatially-varied structure in order to minimize mass transfer limitations.

1. INTRODUCTION

Most pore structure analysis techniques for catalyst supports (adsorption, condensation, mercury porosimetry, TEM/SEM, etc.) are not appropriate for "wet" materials since they require the removal of pore fluid before analysis. Since drying the sample can induce significant, irreversible changes (and is often a

topic of study in its own right), a "non-intrusive" technique is required. The ability to monitor pore structure changes during support processing would be of great utility in the production of catalyst supports with tailored microstructure. In general, changes during processing have been inferred from the pore structure of the final dried material. However, chemistry and structure continue to evolve during processing and the interpretation of how a particular processing parameter affects the final pore structure is not straightforward. The few studies of pore structure evolution during processing use either scattering (SAXS, SANS), thermoporometry, NMR relaxation, or nuclear magnetic resonance imaging (MRI). Also, most pore structure analysis techniques provide structural information which is a spatial average for the entire sample. In fact, significant spatial variations in structure may exist which significantly affect performance. Examples include the possibility of a "skin" on extruded catalysts which may have higher or lower porosity than the bulk of the support or the intended engineering of supports with spatially varying pore structure to minimize mass transfer effects.

2. BACKGROUND

Scattering (x-ray and neutron) primarily provides information on nucleation and growth in solution and/or the structure of the final dried material. The use of scattering for in-situ pore structure analysis suffers from limited length scales, contrast problems, relation of results to pore size, multiple scattering, errors resulting from desmearing, and large analysis costs. However, the approach is quick, allows extraction of all length scales at once, and accesses closed porosity.

Thermoporometry provides pore size information from the comparison of melting and solidification thermograms (i.e., the freezing/melting temperature of pore fluid is a function of pore size) [1,2]. This approach is useful for determining pore size distribution with pores in the size range of 1.5 to 150 nm but suffers from several limitations regarding its use. These include the fact that the pore fluid must be very pure (ie., multiple washes which can change structure), is nonisothermal, requires a pore shape assumption to relate temperature to freezing point, suffers from network/percolation effects, and the volume changes associated with phase change can significantly affect the structure of the sample.

Low-field NMR is often used as a pore structure tool for wet materials and it offers numerous advantages as compared to other techniques including [3,4]:

1) the use of the existing pore fluid as the pore size probe,
2) a large pore size range (<1 nm to > 10 μm),
3) no percolation effects such as porosimetry or nitrogen condensation since the fluid is already in the pores,
4) no pore shape assumption is required for pores larger than several nm,
5) the temperature is held constant during analysis,
6) very high purity fluids are not required,
7) the potential for real-time, on-line measurements of pore structure parameters such as surface area for slurries.
8) sample preparation and analysis time is very rapid (0.5 to 10 minutes).

Disadvantages of the approach include:

1) the technique is a secondary measure in the sense that the fluid-surface interaction parameter must be determined on a solid of known surface area for a given fluid/solid chemestry group,
2) the deconvolution of pore structure information from the relaxation data requires considerable computation.
3) the technique does not work when the sample contains large quantities of magnetic/paramagnetic material.
4) the hydraulic radius of a pore is obtained which is different than what is obtained from porosimetry, etc. except when the pores are cylindrical and monodisperse.

Pore size and surface area information are obtained from the fact that fluid near a surface will undergo spin-lattice (T_1) and spin-spin relaxation (T_2) at a faster rate than for the bulk fluid. From the two-fraction, fast exchange model (see Figure 1), the measured T_1 or T_2 may be related to the pore size by [5]:

$$\frac{1}{T_{1\text{-}2}} = \frac{1}{T_{1\text{-}2_{bulk}}} + \frac{\beta}{r_{pore}} \qquad (1)$$

where the pore size, r_p, is defined as the hydraulic radius in nanometers (twice the pore volume to surface area ratio, 2000 Vp/As, Vp is in cm^3/g, As is in m^2/g).

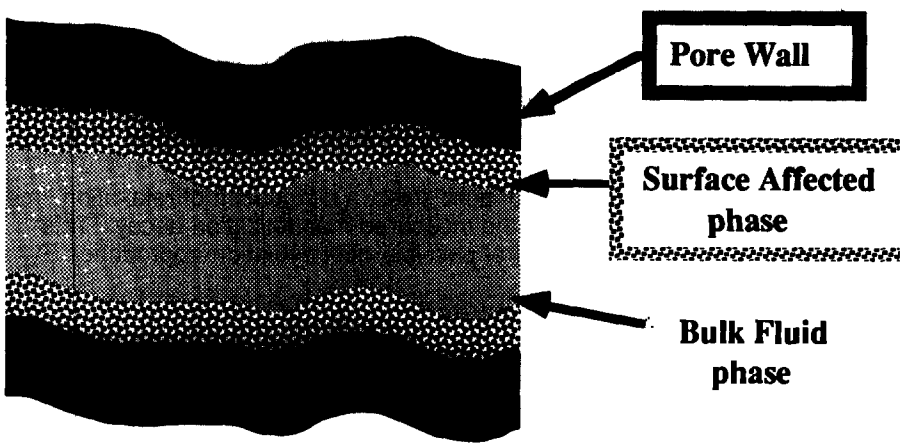

Figure 1 Schematic diagram of pore fluid during a NMR experiment.

When the pore volume is large as compared to the surface area, (i.e., for pore size larger than 3-5 nm) the volume of the surface-affected phase is small and the pore volume to surface area ratio is obtained directly from Equation 1. For smaller pores, assumptions concerning pore geometry and the thickness of the surface-affected phase (typically 0.3 +/- 0.1 nm) are required [6]. We should note that in general, the hydraulic radius and the pore size obtained from other techniques will not be in agreement except when the pores are cylindrical and of the same size. For example, if the pores contain small-scale roughness (<< pore size) which would increase the surface area, the pore size obtained via mercury porosimetry or nitrogen condensation would not be sensitive to this roughness as NMR relaxation pore size would be smaller since it is a surface-sensitive technique. This is both an advantage and a disadvantage and must be considered during data analysis.

From relaxation measurements of fluid in the pores and the bulk fluid, the pore size maybe obtained if the surface interaction parameter, β, is known. β is found by either performing a series of relaxation experiments on partially saturated samples with different moisture contents [7] or by performing relaxation experiments on samples with submonolayer fluid coverage to directly obtain the surface relaxation time [8]. β is a function of temperature, fluid, surface chemistry, and field strength. As the field strength decreases, β increases leading to greater sensitivity to pore size (at the expense of lower signal to noise). Assuming that temperature and field strength are fixed, β for a given fluid-porous solid combination can be found. For high surface area materials, one can dry the sample sufficiently such that the magnitude of the surface relaxation time and the thickness of the surface-affected phase may be measured directly. The more frequent approach is to measure relaxation on an unsaturated sample as the fluid content changes (effectively changing the ratio of bulk to surface-affected phases). If one knows the total surface area of the sample (for example, from nitrogen adsorption), a plot of $1/T_1$ versus the product of M_V (mass of solid per volume of fluid) and surface area should be linear with a slope proportional to β. In general, we have found that β does not vary greatly (i.e. greater than 50%) for a given fluid and a range of solids.

For a solid with a distribution of pore sizes, a distribution of relaxation times exists which must be extracted from the measured magnetization decay. This requires solving Equation 2 via several possible deconvolution approaches [9-11]:

$$M(\tau) = M_0 \int_{T_{1min}}^{T_{1max}} [1-2\exp[-\tau/T_1]]\ f[T_1]\ dT_1 \qquad (2)$$

where $M(\tau)$ is the measured magnetization at different delay times, τ, M_0 is the equilibrium magnetization, and $f[T_1]$ is the desired distribution of relaxation times which is directly related to the desired pore size distribution via Equation 1.

Nuclear Magnetic Resonance Imaging (NMRI) has found wide acceptance in the medical industry but only recently has it been applied to materials science. Part of the reason for this is the cost and experimental complexity but these factors

are more than offset by the types of spatial information (pore size, surface area, chemical state, etc.) which can be obtained in a noninvasive manner. Ackerman and co-workers have applied NMRI to a number of ceramics-related problems including the imaging of pore liquid [10,11]. Hayashi, et al [12] have studied slip-casting of advanced ceramics using NMRI. NMRI has also been applied to study the homogeneity of elastomeric polymers by Chang and Komoroski [13] and Listerud and co-workers [14]. Imaging of pore structure evolution during sol-gel processing has been described by Ewing and co-workers [15].

3. EXPERIMENTAL

Silica gels were prepared from tetraethyl orthosilicate using a two-step, base-catalyzed scheme described by Brinker and co-workers [16]. This system was selected since it yields a fairly broad pore size distribution in both the initial (wet) and final (dried) states and the spatial distribution of pore structure might be similar to that of many materials produced during drying of compliant gels. The pore size distribution and surface area were determined during processing using a 20 MHz NMR and a 180^{o}-τ-90^{o} pulse sequence as described elsewhere [3]. Before drying, samples were aged under various conditions including washing the samples with ethanol to remove the mother liquor (a mixture of water, ethanol, and unreacted TEOS), aging with various pH fluids (water and KOH), and aging in mother liquor for extended time. Samples were dried at ambient conditions for 1 week and then at 383 K. Nitrogen adsorption/condensation (77 K) was used to obtain surface area [5-point BET analysis ($0.05<P/P_0<0.31$, N_2 area=0.162 nm^2)] and volume [1 point, $P/P_0=0.995$] of the dried materials.

In addition to silica gel, model porous solids were produced by packing monodisperse silica spheres. The 130 nm diameter spheres were produced via the hydrolysis and condensation of tetraethyl orthosilicate under basic conditions using the method of Stober et al. [17]. The sphere slurry was filtered, dried, and made into a monolith with a close random packing (porosity = 0.37) by pelleting dried, unagglomerated spheres at 10,000 psia. The structure of these types model porous solids has been previously studied by mercury porosimetry [18] and gas diffusion [19] techniques. A SEM micrograph of a typical fracture surface of these solids is shown in Figure 2.

NMR imaging data was obtained on a modified commercial NMR spectrometer (Bruker CXP-200) at a applied field strength of 4.7 Tesla. The NMR probe was equivalent to that described by Listerrud and co-workers [14]. The magnetic field gradient (40 or 50 gauss/cm) was applied along the direction of the static field. The sample was physically rotated in the probe after each echo. The sample was rotated through 180^{o} using either 94 or 188 echos. The delay time between the pulses and data acquisition was varied to obtain T_1 weighting of the images. Twenty different delay times were employed. The echos were Fourier transformed and corrected to obtain projections, then filtered with a Henning filter [20], and back-projected to give images. The spatial resolution was estimated to

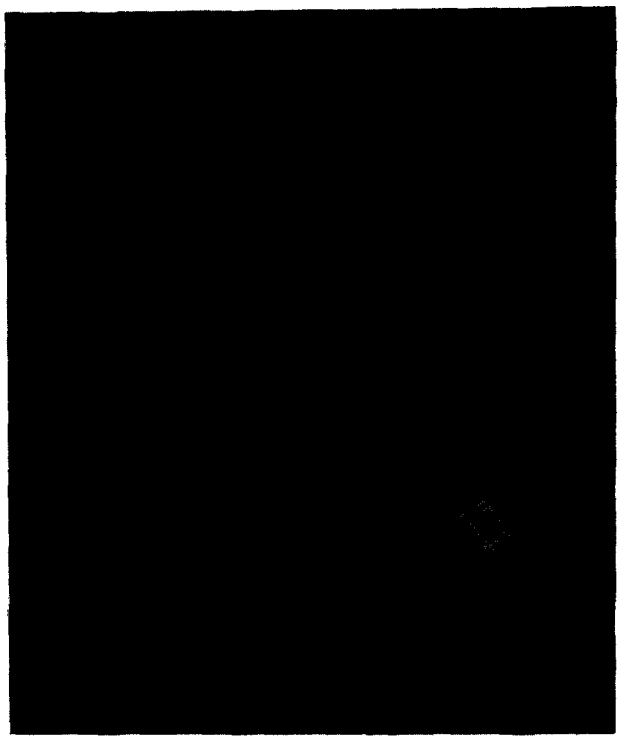

Figure 2 SEM micrograph of a fracture surface for a random packing of 130 nm silica spheres.

be 40 μm per pixel. Details of the experimental imaging procedure have been presented elsewhere [15].

4. RESULTS AND DISCUSSION

Sol-gel processing is an area for which the ability to study pore structure in-situ during wet processing is of great practical importance. By changing processing conditions, the pore size distribution (PSD) of a wet gel can be varied to change further processing steps or the structure and properties of the final dried gel. How the PSD changes during drying is illustrated in Figure 3 for a B2 gel as it dries from mother liquor (~90% ethanol, 10% water) over a one week period. After complete drying at 383 K, the sample was analyzed via N_2 adsorption and condensation and subsequently resaturated with ethanol for NMR analysis. During the initial stages of drying, the large pores disappear as the wet gel shrinks and the entire gel remains saturated. As drying continues, the matrix

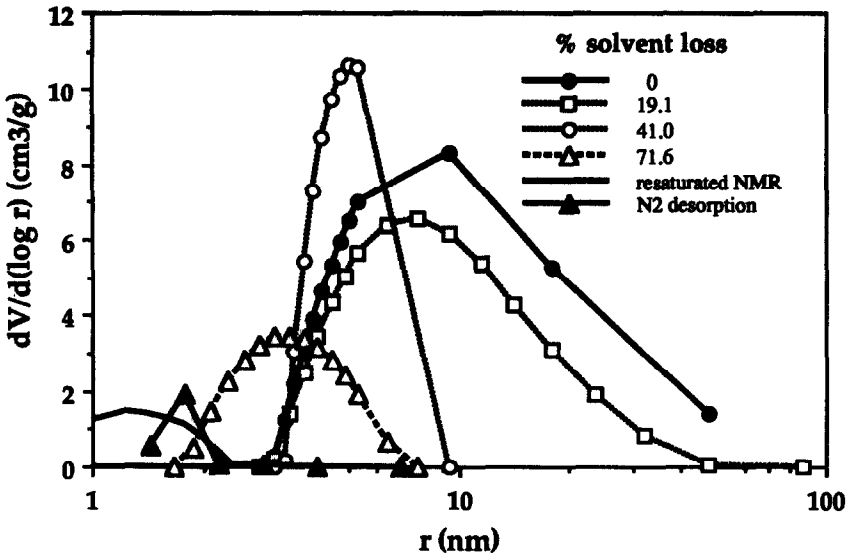

Figure 3 Pore size distribution change during drying of a B2 silica gel. Also included is the PSD of the dried gel by nitrogen condensation and NMR.

stiffens such that the vapor-liquid menisci penetrate the gel. From weight loss and volume measurements, we calculate this to occur for this sample at approximately 75% solvent loss. In general, the amount of solvent lost before the sample is no longer saturated depends upon the solvent surface tension, the wetting angle, the gel matrix strength, and the pore size distribution. We should note that once the porosity of a sample is not completely saturated, one cannot obtain pore size distribution information but can still obtain surface areas. During this final stage of drying, a large decrease in pore size is noted as a result of the large capillary forces in pores less than 10 nm. Although not shown, the surface area is essentially constant at 1200-1500 m^2/g during most of the solvent loss and only during the final stage of drying does it decrease to its final value of ~800 m^2/g. This is probably a result of surface tension-induced condensation reactions of surface Si-OH groups to Si-O-Si with a resultant loss of surface area [21].

The N_2 and NMR pore size results for the dried gel show reasonable agreement. As expected, the NMR PSD exhibits a slightly broader distribution and a mean pore radius which is approximately 50% larger than the adsorption branch. This is a result of two factors: the skewing of condensation results to smaller pore size as a result of network/percolation effects and the fact that NMR obtains the hydraulic radius (i.e., twice the pore volume to surface area) which only agrees with the condensation pore size when the sample contains smooth cylindrical pores of a single size.

The change in pore structure (i.e., porosity, mean pore size, pore size distribution width) was imaged for a B2 gel during drying from mother liquor and during drying of a packing of 130 nm silica spheres saturated with water. Samples

were right cylinders which were imaged along their length to yield radial profiles (images are z-averaged). Figure 4 contains the normalized diameter for both samples during drying as determined from the MRI images as well as with an optical microscope. For the gel, the diameter changed significantly during drying and the diameter as measured from the NMR images was found to agree well with the optically measured dimensions. As expected, the size of the rigid sphere packing did not change significantly according to either measurement technique. The slight differences between the NMR and optical dimensions are probably a result of the sample being slightly off-center in the NMR probe.

From reconstruction of the projections obtained at different angles, two-dimensional images (averaged along the z direction) of porosity are obtained. The spatial distribution of porosity was constant for the sphere packing but the B2 gel exhibited a porosity at the surface approximately 20% higher than at the center of the cylinder. The higher porosity at the surface is the result of the effect of the Pyrex tube on the condensation/gelation process. The most interesting results are presented in Figure 5 which includes radial T_1 profiles, and the radial distribution of X^2 for T_1 (approximately proportional to the width of the pore size distribution) for both the sphere packing (A) and B2 gel (B) before drying. For the sphere packing, both the mean pore size and width of the distribution is uniform across the width of the cylinder. However, for the B2 gel, although the pore size is approximately constant across the cylinder, the width of the distribution changes significantly near the gel surface. The longer T_1 values at the pellet surface are the result of bulk fluid between the pellet surface and the NMR tube.

Although we have not done so, it is fairly straightforward to calculate pore size distributions from X^2. The simplest approach is to assume that the distribution is monodisperse (which previous results support for the two samples employed in this work [8,9]). In that case, by assuming a shape of the pore size distribution (e.g. log normal), an explicit expression relating X^2 and the width of the distribution may be obtained. A more difficult approach which is not restricted to monodisperse distributions but requiring at least 20 different delay times is to invert the relaxation data for each pixel using an approach such as employed for the low field NMR results described in the first part of this paper.

5. ACKNOWLEDGEMENTS

This work has been supported by the UNM/NSF Center for Micro-Engineered Ceramics which is a collaborative effort of the NSF (CDR-8803152), Sandia and Los Alamos National Laboratories, the NMRDI, and the ceramics industry.

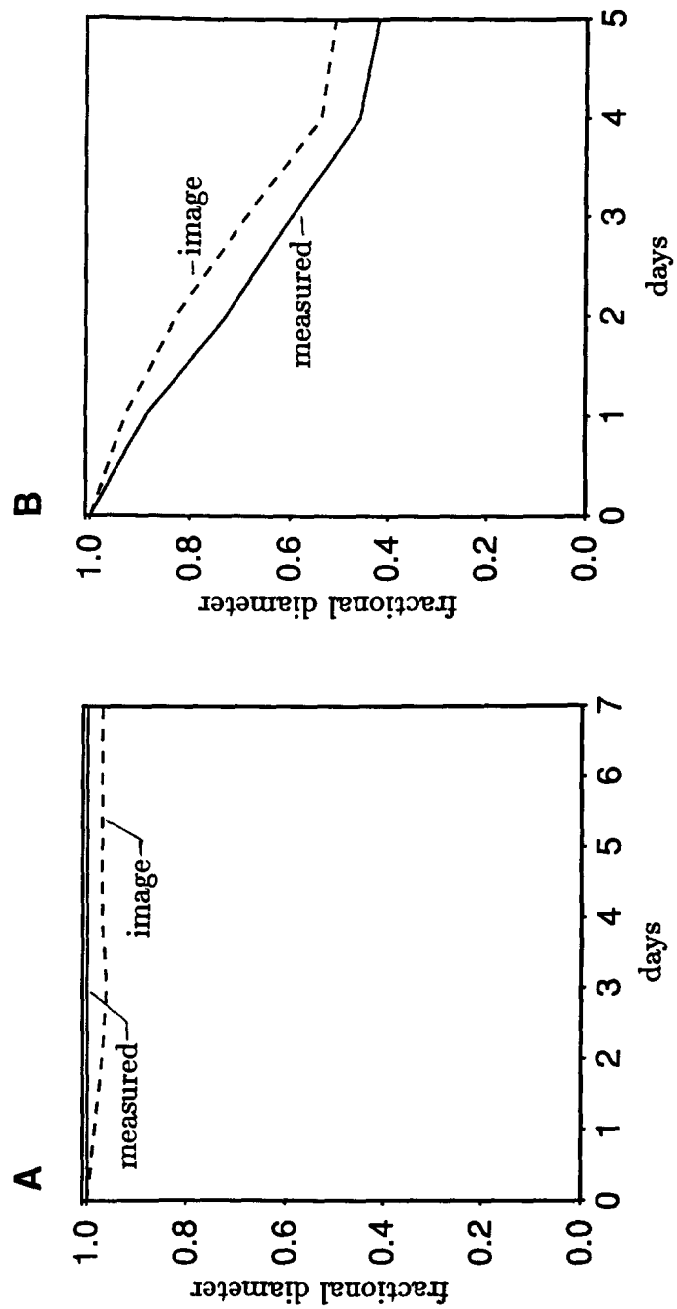

Figure 4 Variation in pellet diameter as a function of drying time for a sphere packing (A) and a B2 silica gel (B) as measured via MRI and optically.

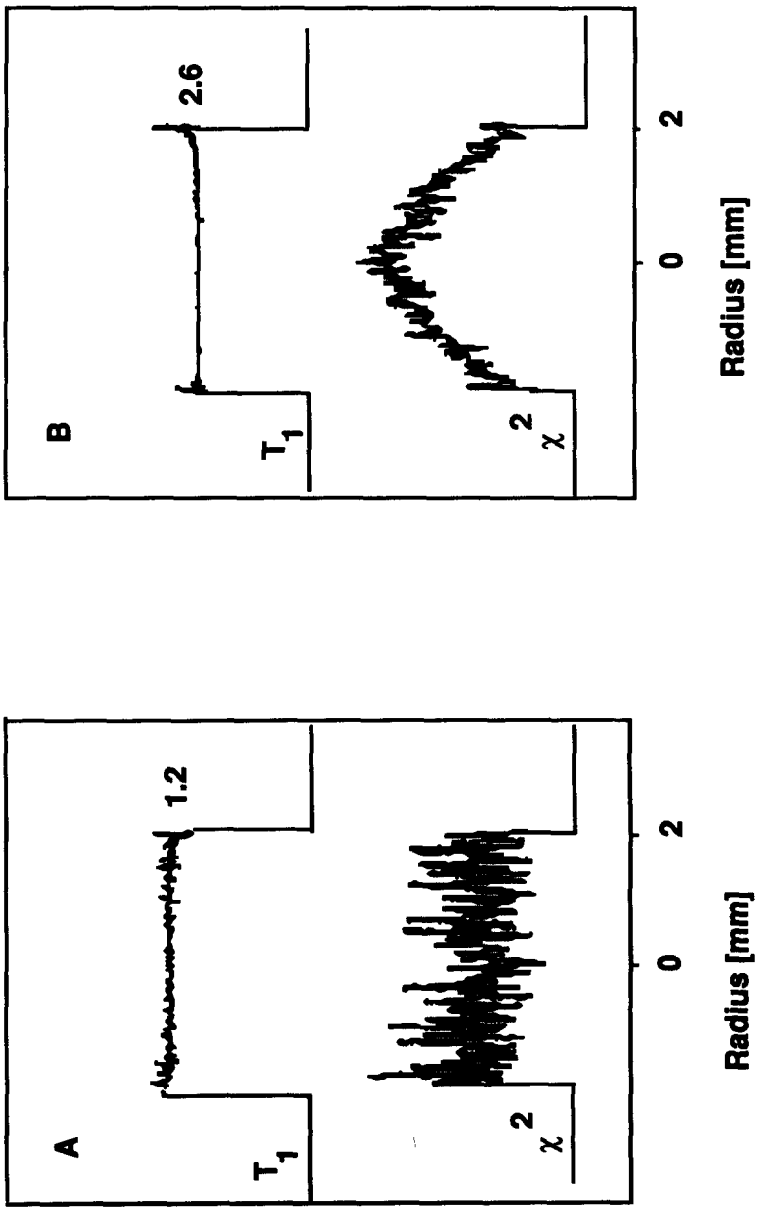

Figure 5 Radial distribution of T1 and standard deviation of T1 for a sphere packing (A) and a B2 silica gel (B).

6. REFERENCES

1. Brun, M., Lallemand, A., Quinson, J., and Eyraud, C., Thermochim. Acta, 21 (1977) 59.
2. Eyraud, C., Quinson, J.F., and Brun, M., in CHARACTERIZATION OF POROUS SOLIDS, Eds. Unger, Rouquerol, Sing, Elsevier, Amsterdam, (1988).
3. Gallegos, D.P., Munn, K., Smith, D.M., and Stermer, D.L., J. Colloid Interface Sci., 119 (1987) 127.
4. Bhattacharja, S., D'Orazio, F., Tarczon, J.C., Halperin, W.P., and Gerhardt, R., J.Am.Ceram.Soc., 72 (1989) 2126.
5. Brownstein, K.R., and Tarr, C.E., J. Mag. Resonance, 26 (1977) 17.
6. Gallegos, D.P., Smith, D.M., and Brinker, C.J., J. Colloid Interface Sci., 124 (1988) 186.
7. Davis, P.J., Gallegos, D.P., and Smith, D.M., Pow. Tech., 53 (1987) 39.
8. Glaves, C.L., Brinker, C.J., Smith, D.M., and Davis, P.J., Chem. Materials, 1 (1989) 34.
9. Gallegos, D.P., Smith, D.M., J. Colloid Interface Sci., 122 (1988) 143.
10. Ellingson, W.A., Ackerman, J.L., Garrido, L., Weyand, J.D., and DiMillia, R.A., Ceram. Eng. Sci. Proc., 8 (1987) 503.
11. Garrido, L., Ackerman, J.L., Ellingson, W.A., and Weyand, J.D., Polymer Preprints, 28 (1988) 97.
12. Hayashi, K., Kawashima, K., Kose, K., and Inouye, T., J. Phys. D: Appl. Phys., 21 (1988) 1039.
13. Chang, C. and Komoroski, R.A., Macromolecules, 22 (1989) 600.
14. Listerud, J.M., Sinton, S.W., and Drobney, G.P., Anal. Chem., 61 (1989) 23A.
15. Ewing, B., Davis, P.J., Majors, P., Drobny, G.P., Smith, D.M., and Earl, W.L., in CHARACTERIZATION OF POROUS SOLIDS II, Eds. Unger, Rouquerol, Sing, Elsevier, Amsterdam, (1991).
16. Brinker, C.J., Keefer, K.D., Schaefer, D.W., Ashley, C.S., J. Non-Cryst. Solids, 48 (1982) 47.
17. Stober, W., Fink, A., Bohn, E., J. Colloid and Interface Sci. , 26 (1968) 62.
18. Smith, D.M. and Stermer, D.L., J. Colloid and Interface Sci. , 111 (1986) 160.
19. Huizenga, D.G. and Smith, D.M., AIChE Journal, 32 (1986) 1.
20. Chesler, D.A., and Riederer, S.J., Phys. Med. Biol., 20 (1975) 632.
21. Deshpande, R., Smith, D.M., and Brinker, C.J., J.Non-Cryst. Solids, submitted.